Research Results in Pharmacology

Research Results in Pharmacology 12(3): 18–34
UDC 615.1/.4:546.47
DOI 10.18413/rrpharmacology.12.1240

Research Article

Pharmacokinetic parameters of a zinc complex with N-allylimidazole

Victoria S. Babasieva[1], Vladislav N. Turenko[1,2], Andrey R. Grabeklis[3], Dmitry M. Lyapunovsky[3], Anatoly V. Skalny[3], Vladimir S. Tyurin[4], David E. Bagaev[1,2], Victoria G. Krasnyanskaya[2], Galina F. Vasilenko[2], Obinna Ikebunwa[1,5], Valery V. Smirnov[1,2], Svetlana A. Lebedeva[1,3,6]

1 Institute of Pharmacy, Sechenov First Moscow State Medical University (Sechenov University); 8-2 Trubetskaya St., Moscow 119048 Russian Federation;
2 Allergy and Immunology Research Centre FMBA of Russia; 24 Kashirskoye Shosse, Moscow 115522 Russian Federation;
3 People's Friendship University of Russia named after Patrice Lumumba (RUDN University); 6 Miklukho-Maklaya St., Moscow 117198 Russian Federation;
4 Frumkin Institute of Physical Chemistry and Electrochemistry, Russian Academy of Sciences; 31 Leninsky Prospekt, Bldg 4, Moscow, 119071 Russian Federation;
5 Department of Pharmacology and Toxicology, Michigan State University; 1355 Bogue St., East Lansing, Michigan 48824 USA;
6 Scientific Center of Genetics and Life Sciences, Sirius University of Science and Technology; 1 Olimpiysky Prospekt, Sirius Federal Territory, Krasnodar Krai, 354340 Sirius, Russian Federation.

Corresponding author: Svetlana A. Lebedeva (lebedeva502@yandex.ru)

Academic editor: Tatyana Avtina ♦ **Received** 15 July 2026 ♦ **Accepted** 15 September 2026 ♦ **Published** 25 September 2026

Citation: Babasieva VS, Turenko VN, Grabeklis AR, Lyapunovsky DM, Skalny AV, Tyurin VS, Bagaev DE, Krasnyanskaya VG, Vasilenko GF, Ikebunwa O, Smirnov VV, Lebedeva SA (2026) Pharmacokinetic parameters of a zinc complex with N-allylimidazole. Research Results in Pharmacology 12(3): 18–34. https://doi.org/10.18413/rrpharmacology.12.1240

Abstract

Introduction: Zinc is an essential trace element with well-known physiological functions. Although various zinc salts are available, novel zinc complexes with organic ligands remain of pharmacological interest. Pharmacokinetic studies are essential to clarify the contribution of the zinc ion and organic ligand to their biological activity.

Materials and Methods: The pharmacokinetics of bis(N-allylimidazole) zinc diacetate (ALL) components were studied in 66 BALB/c mice. The compound was administered once intraperitoneally at 25 mg/kg. Blood, brain, liver, pancreas, kidneys, and spleen were collected at 0, 0.083, 0.25, 0.5, 1, 1.5, 2, 3, 4, 6, and 24 h, with 6 animals per time point. N-allylimidazole was quantified using a validated HPLC-MS/MS method, while zinc was determined by atomic absorption spectrometry.

Results and Discussion: ALL likely dissociates into N-allylimidazole and zinc under physiological conditions, resulting in distinct pharmacokinetic profiles. N-allylimidazole was detected in all tissues, including the brain. The Tmax for most tissues was 0.25 h, indicating rapid systemic distribution. The highest concentration was observed in the kidneys (Cmax 7907.58 µg/g), suggesting their involvement in ligand excretion. In the liver, N-allylimidazole showed prolonged retention, with a $T_{1/2}$ of 14.5 h and AUC(0–24) of 11168.41 µg·h/mL. After correction for endogenous zinc, the highest zinc concentrations were detected in the liver (60.21 µg/g), pancreas (57.52 µg/g), and spleen (54.80 µg/g).

Conclusion: ALL administration resulted in rapid systemic distribution of both components. N-allylimidazole penetrated highly perfused tissues, including the brain and kidneys, whereas zinc accumulated in the liver, pancreas, and spleen. Distinct tissue distribution and elimination profiles, together with equilibrium calculations, support complete *in vivo* dissociation of the complex.

Graphical Abstract

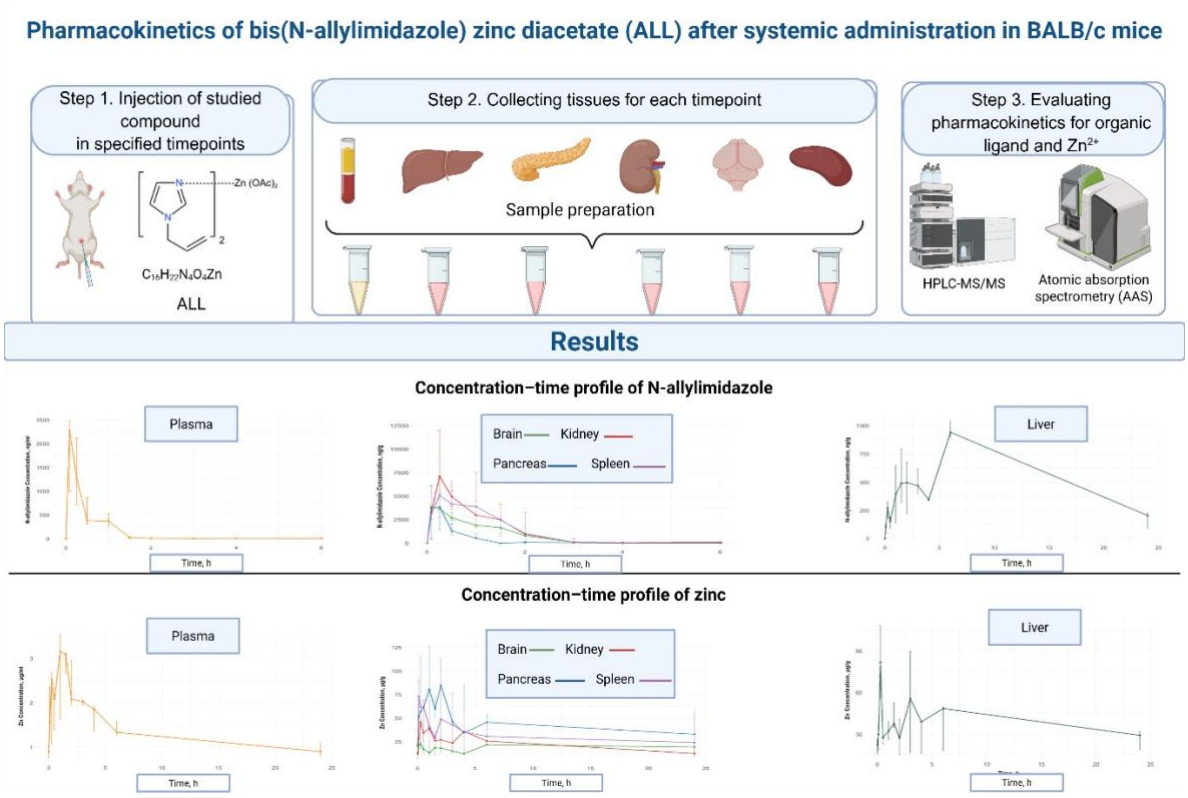

Keywords

zinc; N-allylimidazole; pharmacokinetics; HPLC-ESI-MS/MS; atomic absorption spectrometry

Introduction

Zinc is an essential trace element required for normal cellular, tissue, and organ function. It is incorporated into nearly 3,000 proteins and 300 enzymes, contributing to structural stability and facilitating interactions with diverse biomolecules. Beyond its catalytic role, zinc stabilizes protein domains and membrane complexes and regulates gene expression, cell proliferation, differentiation, apoptosis, and immune responses.

Zinc also plays a central role in intracellular signaling. Zn^{2+} influx from the extracellular space or release from intracellular stores can act as a primary messenger by modifying cellular responses, whereas increases in cytosolic Zn^{2+} function as a secondary messenger. Changes in cytosolic Zn^{2+} modulate kinases, phosphatases, transcription factors, and other signaling proteins, thereby regulating pathways involved in growth, inflammation, antioxidant defense, tissue repair, and stress adaptation.

In adults, total body zinc is approximately 1.5–3 g, with the largest fractions in skeletal muscle and bone, and significant pools in the skin, liver, prostate, and blood cells. In plasma, most zinc is protein-bound, predominantly to albumin, whereas the free fraction is minimal. The bound pool governs zinc transport and tissue distribution, while the small free fraction supports rapid exchange and signaling.

Intracellular free zinc concentrations are maintained at non-toxic picomolar levels (Kocyła et al. 2018) through binding to metallothioneins (MTs) and sequestration in specialized storage compartments termed zincosomes. Zinc homeostasis is primarily regulated by two transporter families: 14 importers of the SLC39 family (ZIP), which increase cytosolic zinc levels, and 10 exporters of the SLC30 (ZnT) family, which reduce cytosolic zinc promoting efflux or

sequestration into organelles such as the Golgi apparatus and lysosomes (Kimura and Kambe 2016; Lin et al. 2017).

Zinc fingers (ZNFs) are compact domains stabilized by coordination of a zinc ion with cysteine and/or histidine residues. Many ZNFs mediate sequence-specific binding to nucleic acid motifs, enabling precise transcriptional regulation and also participate in post-translational signaling cascades. Their functional diversity encompasses embryonic development, cell differentiation, maintenance of genomic stability, and immune regulation. Dysregulation or mutation of ZNFs is associated with inherited disorders and cancer; for example, knockdown of ZNF307 enhances hepatocellular carcinoma proliferation and invasiveness by reducing apoptosis-related proteins such as caspase-3 and BCL-2 (Liang et al. 2017).

ZNFs are also critical regulators of pluripotency, differentiation, and somatic cell reprogramming (Qian and Wu 2025). In neuronal development, ZNF18 interacts with promoters of genes involved in neuronal maturation and dopamine secretion (Park et al. 2025). Dysregulation and aggregation of zinc-binding proteins may contribute to neurodegenerative disorders, including Parkinson's disease (Brahmachari et al. 2019), while regulatory mutations in ZNF512B have been implicated in amyotrophic lateral sclerosis (Jiang et al. 2021).

As a cofactor for more than 300 enzymes (Costa et al. 2023), zinc is involved in a wide range of physiological processes and is the only metal present across all enzyme classes (Andreini et al. 2006). Structurally, zinc stabilizes protein secondary and tertiary structures, ensuring proper folding and activity of oligomeric enzymes (Thompson 2022). Representative zinc-dependent enzymes include carbonic anhydrase, alcohol dehydrogenase, Cu/Zn-superoxide dismutase, matrix metalloproteinases, and histone deacetylases (Hou et al. 2021).

Chronic zinc deficiency, whether inherited or acquired, leads to clinically significant disorders. Acquired deficiency may result from inadequate intake, malabsorption, increased requirements, or excessive losses. Hereditary zinc deficiency is most commonly associated with mutations in SLC39A4 (ZIP4) and manifests as alopecia, diarrhea, and acrodermatitis enteropathica (Stiles et al. 2024). Severe deficiency syndromes, such as Prasad's syndrome, are characterized by growth retardation, delayed puberty or hypogonadism, iron-deficiency anemia, and hepatosplenomegaly (Demirel et al. 2011).

The prevalence of zinc deficiency is estimated at 10-20% depending on the region (Skalny et al. 2022). Because the body lacks substantial zinc storage capacity, regular dietary intake is essential. Treatment of acquired deficiency typically involves oral zinc supplementation, including zinc oxide and zinc salts such as acetate, gluconate, aspartate, orotate, and sulfate. Zinc oxide exhibits lower bioavailability, particularly when taken on an empty stomach, due to its limited solubility compared with other formulations (Wegmüller et al. 2014).

Zinc acetate not only corrects deficiency but also exhibits antiviral activity against hepatitis A virus and may reduce disease progression (Gómez-Zorrilla et al. 2025; Kanda et al. 2025). Zinc acetate lozenges have been shown to shorten the duration of acute respiratory viral infections (Hemilä et al. 2016). In experimental models of hepatocellular carcinoma, zinc acetate induces apoptosis (Hashimoto et al. 2022). In diabetic rat models, zinc acetate combined with caffeic acid improves metabolic parameters, including body weight, insulin secretion, and glycogen storage (Matowane et al. 2023). Zinc sulfate has demonstrated protective effects in renal ischemia–reperfusion injury by reducing apoptosis and pyroptosis (Guo et al. 2024), preserving ovarian function (Dong et al. 2023), and attenuating muscle atrophy by inhibiting excessive autophagy (Yu et al. 2025).

Despite their clinical use, inorganic zinc salts are limited by relatively low bioavailability and gastrointestinal adverse effects, whereas organic zinc complexes generally exhibit improved tolerability and pharmacokinetic profiles.

Zinc complexes with N-alkenylimidazoles are of particular interest due to their diverse pharmacological activities. Acyzol (bis(N-vinylimidazole) zinc diacetate), used as an antidote for carbon monoxide and combustion product poisoning, exhibits antihypoxic, antioxidant, hepatoprotective, cardioprotective, and immunomodulatory properties (Shakhmardanova and Galenko-Yaroshevskii 2017; Aliev et al. 2019; Parshina et al. 2019).

Pilim-1 (bis(N-isopropenylimidazole) zinc diacetate) and ALL bis(N-allylimidazole) zinc diacetate) demonstrate antihypoxic, antimicrobial, and regenerative effects (Shakhmardanova and Galenko-Yaroshevskii 2017; Lebedeva et al. 2023). Topical application accelerates wound healing and improves tissue architecture more effectively than reference drugs (Lebedeva et al. 2023). Pilim-1 additionally exhibits anti-inflammatory, analgesic, and antiulcer effects in animal models (Galenko-Yaroshevsky et al. 2024a, 2024b). Antitumor activity has also been reported for zinc chloride complexes with N-alkenylimidazoles (Tyurin et al. 2026).

The pharmacological activity of metal complexes depends on their chemical structure and pharmacokinetic properties, including absorption, distribution, metabolism, and excretion. For

zinc complexes, biological effects are closely related to coordination state, lipophilicity, and membrane permeability. A key consideration is stability in biological media: whether the coordination structure remains intact, whether the compound reaches target tissues, and whether therapeutically effective concentrations are maintained. If dissociation occurs, biological effects may result from free zinc ions and ligands rather than the intact complex, potentially altering efficacy and safety due to excess free zinc. Pharmacokinetic studies are therefore essential to determine whether N-alkenylimidazole ligands enhance bioavailability, prolong systemic circulation, or promote selective tissue accumulation.

Such data are critical for elucidating mechanisms of action, optimizing dosing strategies, and supporting further development of these compounds as therapeutic agents. Accordingly, this study aims to characterize the pharmacokinetic parameters of bis(N-allylimidazole) zinc diacetate (ALL) following systemic administration in BALB/c mice.

Materials and Methods

Investigated compound

The zinc complex ALL was synthesized at the A.E. Favorsky Irkutsk Institute of Chemistry, Siberian Branch of the Russian Academy of Sciences (Russia).

Stability constant calculations

The constant of formation of the zinc complex ALL was calculated ab initio with density functional theory (DFT) using Gaussian 16 software package (Frisch, et al. 2016). The thermochemical parameters were calculated using the MN15 functional in conjunction with 6-311+G(2df,2p) basis set. The solvent (water) effects were accounted for by the polarizable continuum model (PCM).

Animals

The study was conducted in 66 BALB/c mice weighing 20–22 g. Animal housing and handling were carried out in accordance with GOST 33044–2014 “Principles of Good Laboratory Practice,” approved by Order No. 1700-st of the Federal Agency for Technical Regulation and Metrology (November 20, 2014). The experimental protocols were approved by the Local Ethics Committee of Sechenov University (Minutes No. 03-26 of 6 February 2026).

Study design

The study design is presented in Figure 1.

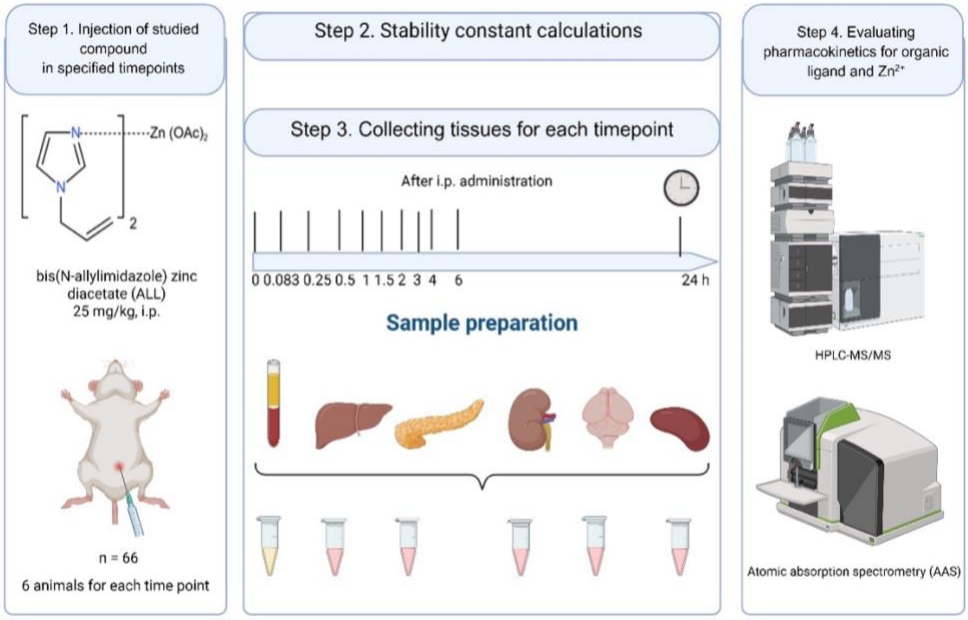

Figure 1. Pharmacokinetic Parameters of a Zinc Complex with N-Allylimidazole study design.

The complex compound was administered intraperitoneally (i.p.) at a dose of 25 mg/kg. After the animals were euthanized by cervical dislocation, the following biological samples were collected: blood, brain, liver, pancreas, kidneys, spleen at the following time points

0, 0.083, 0.25, 0.5, 1, 1.5, 2, 3, 4, 6, 24 h with 6 animals for each time point. After collection, blood samples were centrifuged to obtain plasma.

Homogenization procedure

To perform a quantitative assessment of the drug content in the biological material, sample preparation was first carried out in order to obtain a purified organic extract. Each organ was placed in an individual tube containing ceramic beads, to which a volume of saline corresponding to the organ was added – 1.5 mL for the brain, pancreas, spleen, and kidneys, and 4 mL for the liver – and was homogenized using a FastPrep-24 homogenizer. Homogenization occurred through the collision of the special beads, following the ball-mill principle. Centrifugation of the sample took place simultaneously.

Sample preparation for N-allylimidazole

After homogenization was complete, the tubes together with their contents were left to settle for 10 minutes – yielding the homogenate. Next, 350 μL of the homogenate was transferred into a separate tube, one and a half volumes of acetonitrile (525 μL) were added, and the contents were mixed using a laboratory vortex and centrifuged for 10 minutes at 12,000 rpm. The clear, colorless supernatant was transferred into a clean 1.5 mL tube. The resulting extracts were stored until analysis at -20 °C.

350 μL of the blood plasma was transferred into a separate tube, one and a half volumes of acetonitrile (525 μL) were added, and the contents were mixed using a laboratory vortex and centrifuged for 10 minutes at 12,000 rpm. The clear, colorless supernatant was transferred into a clean 1.5 mL tube. The resulting extracts were stored until analysis at -20 °C.

Sample preparation for Zn^{2+}

The homogenate was mixed on a laboratory vortex to the greatest possible homogeneity; the sample weight was approximately the same for all sample types and amounted to ~ 0.4 ± 0.05 g. Next, concentrated nitric acid (70%, "Komponent-Reaktiv", chemically pure grade) was added to the weighing bottles in a volume of 1 mL, and high-temperature mineralization of the samples was carried out in a microwave oven for ~ 20 minutes using two sequential heating modes (12 minutes at 560 W, then 8 minutes at 400 W). The resulting mineralizate was quantitatively transferred from the weighing bottles into disposable polypropylene tubes and diluted with deionized water to a final volume of 15 mL.

Quantitative determination of N-allylimidazole by HPLC-MS/MS

For the chromatographic separation and determination of N-allylimidazole in plasma samples, a system consisting of an Agilent Infinity II 1260 high-performance liquid chromatograph equipped with a gradient pump, column thermostat, degasser, autosampler, and an Agilent 6490 tandem quadrupole mass spectrometer (MS/MS) was used.

The following reagents and materials were used: acetonitrile (HPLC grade ≥99.9%), formic acid (≥99%), purified water (Milli-Q) for HPLC, N-allylimidazole reference standard, and intact plasma samples.

To prepare mobile phase (MP) A, 2.0 mL of formic acid were placed into a 1000 mL volumetric flask, the volume was made up to the mark with acetonitrile, and mixed. To prepare MP B, 2.0 mL of formic acid were placed into a 1000 mL volumetric flask, the volume was made up to the mark with purified water, and mixed.

To validate the method and further quantify, model reference standards prepared by mixing 500 μL of the corresponding working solution with 500 μL of intact plasma were used, after which sample preparation was carried out as described above. The concentrations of the obtained standard calibration solutions corresponded to the following concentration range: 1, 5, 10, 25, 50, 100, 250, 500, 1000, 2500 ng/mL. ESI-MS/MS parameters were optimized to achieve the highest sensitivity of the method: precursor ion 109.1; product ion 41.2; gas temp 350 °C; gas flow 7 L/min; sheath gas flow 8 L/min; ion spray voltage 5500; collision energy 25.

Quantitative determination of Zn^{2+} by atomic absorption spectrometry (AAS)

AAS analysis of the samples for Zn content was performed using a KVANT.Z atomic absorption spectrophotometer (CORTEC, Russia) equipped with an electrothermal atomizer. The analytical signal was measured in the absolute signal intensity registration mode. To construct the calibration curve, working standard metal (Zn) solutions were used, prepared by appropriate dilution of the primary State Standard Sample (SSS) solutions. As the control material, the certified reference material GBW07601 (Shanghai Institute of Nuclear Research, PRC) was used, prepared according to the same sample preparation procedure as the test samples. For atomization, a graphite cuvette with a non-pyrolytic coating was used. The light source was an

"LT-6M" hollow-cathode lamp manufactured by CORTEC; the wavelength for Zn measurements in the experiment was 307.6 nm.

A 10 µL aliquot, with the addition of the chemical modifier $Pd(NO_3)_2$ (Merck, Germany) for improved sensitivity to zinc.

Pyrolysis stage III – 400 °C, atomization stage 1810 °C. Lamp current: 20 mA.

At the end of the pyrolysis stage and the beginning of the atomization stage, the inert gas (argon) flow was stopped. Dosing of microvolumes of the solutions into the furnace was carried out using an automatic dispenser.

Statistical analysis

Statistical analysis was performed in R, version 4.4.3, using the Bear package for non-compartmental analysis. The following pharmacokinetic parameters were calculated: C_{max}, T_{max}, λz, $T_{1/2}$, AUC_{0-t}, $AUC_{0-\infty}$, MRT_{0-t}, and $MRT_{0-\infty}$.

Results

Development and validation of the HPLC-MS/MS method

The methods were validated in accordance with the rules for conducting bioequivalence studies of drugs within the Eurasian Economic Union (approved by decision No. 85 of the Council of the Eurasian Economic Commission of 03 November 2016) for the following validation parameters: specificity, limit of quantification, linearity, analytical range, precision (repeatability), accuracy, transfer effect, matrix effect, stability. All obtained values complied with the regulatory documentation requirements.

The HPLC-ESI-MS/MS method was developed on a chromatographic column for ultra HPLC "Waters Symmetry C18", C18, 250 × 4.6 mm, 5 µm. An Eclipse Plus C18 2.1 × 12.5 mm, 5 µm protective column was used to protect the main column from biological sample related substances. The MP composition was selected as follows to obtain a positively charged parent ion of N-allylimidazole: MP A 0.2% formic acid in purified water, MP B 0.2% formic acid in acetonitrile. The gradient program was as follows: 5% B (0.00–1.00 min), 5–70% B (1.00–4.00 min), 70% B (4.00–4.50 min), 70-5% B (4.50–5.00 min); the flow rate was set at 0.5 mL/min. The column temperature was 40 °C, injection volume 10 µL. To select the multiple reaction monitoring transition for N-allylimidazole detection, the mass spectrum was recorded and the most intense product ion 41.2 was selected (Fig. 2).

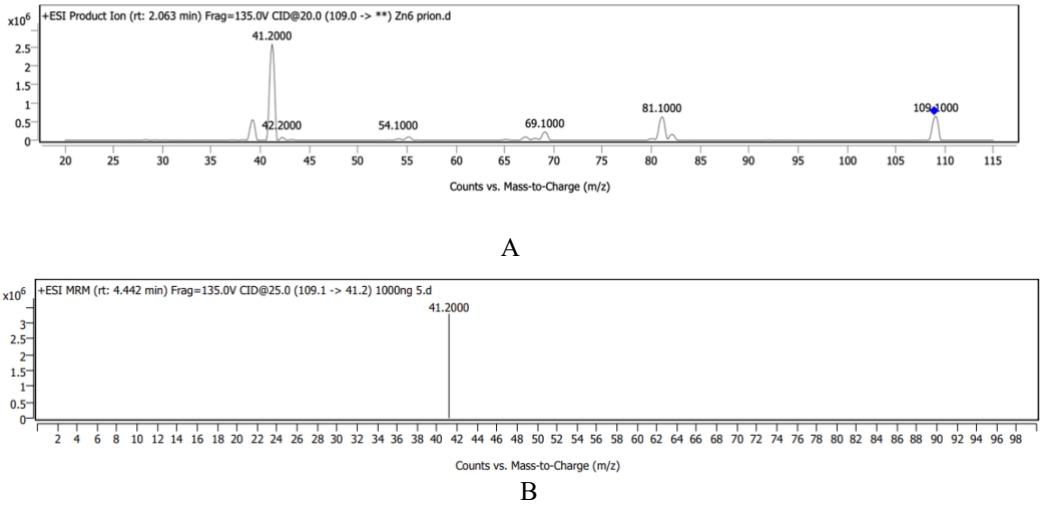

Figure 2. Mass spectrum of N-allylimidazole (**A**) and it`s multiple reaction monitoring transition (**B**).

ESI-MS/MS parameters were optimized to achieve the highest sensitivity of the method: precursor ion 109.1; product ion 41.2; gas temp 350 °C; gas flow 7 L/min; sheath gas flow 8 L/min; ion spray voltage 5500; collision energy 25.

The retention time of N-allylimidazole was approximately 4.4 min, and typical chromatograms of blank and blood plasma are shown in Figure 3.

Linearity was assessed over the range of 1–2500 ng/mL using calibration standards prepared at ten concentration levels (Fig. 3). Lower limit of quantification (LLOQ) and upper limit of quantification (ULOQ) were 1 and 2500 ng/mL, respectively.

For each level, the concentration was back-calculated from the calibration curve, and the deviation from the nominal value was determined (Table 1).

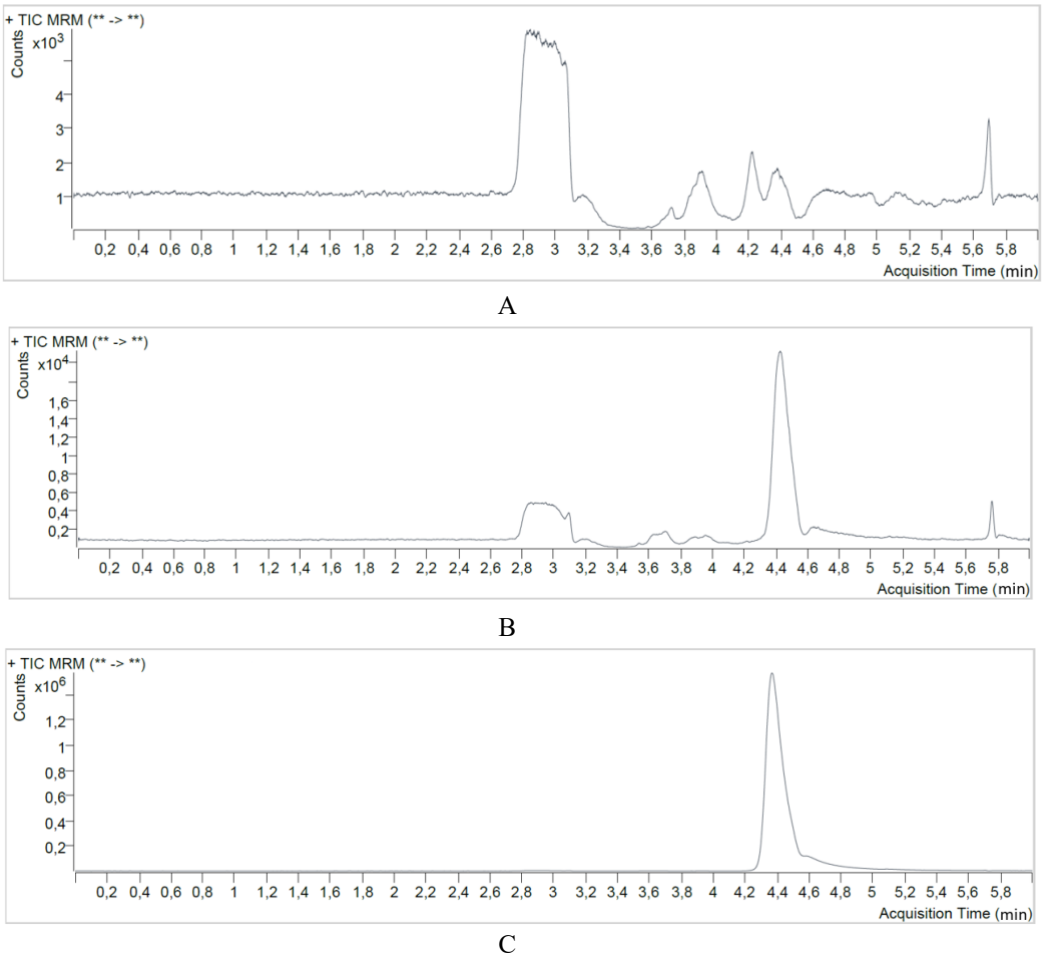

Figure 3. Typical high performance liquid chromatography with electrospray ionization tandem mass-spectrometry chromatograms of blank (**A**), blood plasma with the study drug at concentrations of 1 ng/mL (LLOQ) (**B**) and 500 ng/mL (**C**).

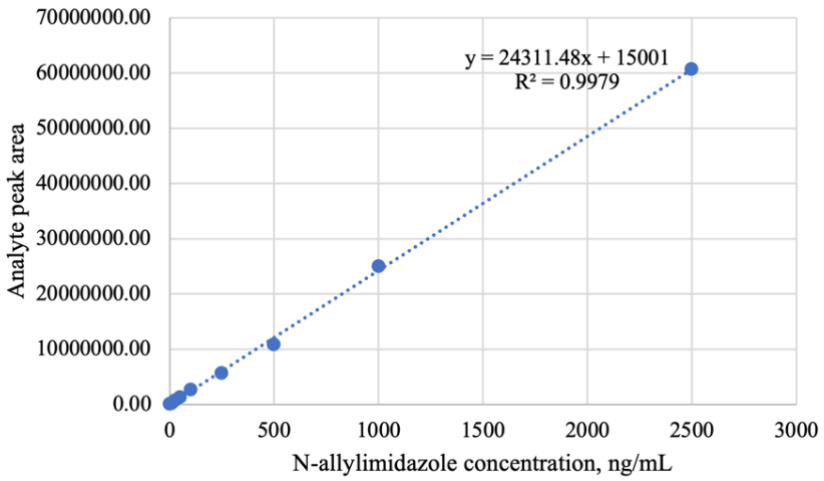

Figure 4. Calibration curve for the determination of N-allylimidazole from validation cycle 1.

The deviation of the back-calculated concentrations did not exceed ±15% at any level (±20% at the lower limit of quantification), thereby satisfying the acceptance criteria of Decision No. 85.

Accuracy and precision were determined at five concentration levels (1, 5, 500, 1000 and 2500 ng/mL) with five replicates per level in each of three analytical runs. Precision was

expressed as the relative standard deviation (RSD) and accuracy as the relative bias from the nominal concentration (Table 2).

Table 1. Linearity of the HPLC-MS/MS method for N-allylimidazole: mean back-calculated concentrations of the calibration standards and their deviation from nominal values

Nominal concentration, ng/mL	Run	Mean back-calculated concentration, ng/mL	Deviation from nominal, %
1	1	0.93	-7.32
	2	0.93	-7.00
	3	0.95	-4.67
5	1	4.67	-7.22
	2	4.67	-6.53
	3	4.71	-5.80
10	1	10.61	+6.08
	2	10.11	+1.07
	3	10.09	+0.90
25	1	24.16	-3.28
	2	23.97	-4.12
	3	24.32	-2.71
50	1	50.66	1.32
	2	50.63	1.27
	3	50.09	0.17
100	1	109.53	9.53
	2	108.89	8.89
	3	105.35	5,35
250	1	234.57	-6.17
	2	230.35	-7.86
	3	240.87	-3.65
500	1	481.48	-3.70
	2	484.96	-3.01
	3	483.68	-3,26
1000	1	1029.14	2.91
	2	1009.69	0.97
	3	1022.17	2.22
2500	1	2494.00	-0.24
	2	2514.11	0.56
	3	2521.16	0.85

Table 2. Within-run and between-run accuracy and precision of the HPLC-MS/MS method for N-allylimidazole (five replicates per run; n = 30 for the between-run estimate)

Nominal concentration, ng/mL	Run	Measured concentration, mean, ng/mL	SD, ng/mL	RSD, %	Accuracy, %
1	Run 1	0.8991	0.0489	5.43	−10.09
	Run 2	0.9092	0.0422	4.64	−9.08
	Run 3	0.8936	0.0137	1.54	−10.64
	Between-run	0.9007	0.0359	3.99	−9.93
5	Run 1	4.6094	0.3596	7.80	−7.81
	Run 2	4.7674	0.3765	7.90	−4.65
	Run 3	4.9221	0.1857	3.77	−1.56
	Between-run	4.7663	0.3237	6.79	−4.67
500	Run 1	519.4690	21.0033	4.04	+3.89
	Run 2	515.0226	15.1179	2.94	+3.00
	Run 3	507.6513	12.0704	2.38	+1.53
	Between-run	514.0476	16.0753	3.13	+2.81
1000	Run 1	894.2876	24.4565	2.73	−10.57
	Run 2	919.7362	44.6340	4.85	−8.03
	Run 3	932.0455	45.9653	4.93	−6.80
	Between-run	915.3564	40.1074	4.38	−8.46
2500	Run 1	2558.4443	50.8051	1.99	+2.34
	Run 2	2536.2342	36.2342	1.43	+1.45
	Run 3	2514.8543	30.1744	1.20	+0.59
	Between-run	2536.5109	41.3773	1.63	+1.46

In all cases, the within-run and between-run precision (RSD) did not exceed 8%, and the bias remained within ±15% of the nominal value, in accordance with the acceptance criteria of Decision No. 85. LLOQ of the method was determined based on the data of the calibration curve, accuracy and precision. The minimum concentrations of N-allylimidazole in blood plasma in the analytical ranges for which quantitative determination of N-allylimidazole with RSD and accuracy values of no more than 20% is possible were taken as the basis for the LLOQ. The lower limit of the quantitative determination of the method was 1 ng/mL for N-allylimidazole.

During the assessment of the transfer effect, samples of ULOQ, intact blood plasma samples and LLOQ were sequentially analyzed. On chromatograms of intact blood plasma samples, the N-allylimidazole area values corresponded to the acceptability criterion (Analyte transfer ≤ 20% of LLOQ).

To determine the matrix effect in the quantitative analysis of N-allylimidazole, the matrix effect coefficient (ME, %) was calculated, which is expressed as the ratio of the peak of the analyte added to the intact plasma (matrix) to the peak area of a standard calibration solution without a matrix. All solutions were sampled using the method described above. The effect of the matrix was calculated at 1 ng/mL and 2500 ng/mL (Table 3).

Table 3. Calculation of the effect of the biological matrix on the quantitative determination of N-allylimidazole in blood plasma at the levels of LLOQ and ULOQ

Nominal concentration, ng/mL	ME, %	Mean, %	SD	RSD, %
1	91.24	91.57	9.19	10.04
	91.38			
	92.70			
	100.96			
	98.48			
	74.68			
2500	107.81	104.52	3.01	2.88
	102.07			
	107.58			
	100.42			
	103.57			
	105.71			

The following types of stability were confirmed: stability of prepared samples at ambient temperature and autosampler temperature, stability during triple freezing and defrosting, stability during deep freezing. The relative error values obtained correspond to the acceptability criterion (in the range from -15% to +15%) (Table 4).

Table 4. Conditions and period of storage of N-allylimidazole samples for stability assessment

Storage conditions	Period of storage	Result, % from nominal	Compliance with the acceptability criterion (relative error ≤ 15%)
At ambient temperature	24 h	LLOQ 89,1% ULOQ 113%	Yes
At the autosampler thermostat temperature of 2–8 °C	24 h	LLOQ 87,3% ULOQ 106%	Yes
Freezing at –80 °C, thawing at ambient temperature in three replicates	At least 36 hours in the frozen state, and at least 6 hours in the thawed state	LLOQ 87,7% ULOQ 95%	Yes
At –80 °C	96 h	LLOQ 89,3% ULOQ 97,1%	Yes

Partial validation was performed for each biological tissue sample, including confirmation of specificity and linearity for model samples prepared using homogenates of the corresponding organs. For brain, liver, pancreas, kidneys, spleen the following correlation coefficients were obtained 0.994, 0.998, 0.996, 0.995, 0.999.

Validation of the AAS method for zinc quantification

For validation of the AAS method, cross-validation was performed against a previously validated ICP-MS method (Miroshnikov et al. 2020). Additionally, to demonstrate the suitability of the

analytical method for the purposes of this study, partial validation was performed using spiked samples containing the biological matrix under study and a known added amount of certified zinc reference material (GBW07601, Shanghai Institute of Nuclear Research, PRC). During the validation of the AAS method, the following analytical parameters were determined: specificity, linearity, precision (repeatability), accuracy. Partial validation data for plasma is shown in Figure 5 and Table 5 below. Linearity was estimated for the concentration range from 1 to 15 µg/mL. For all the studied biological samples, the correlation coefficient was within the range of 0.991–0.995.

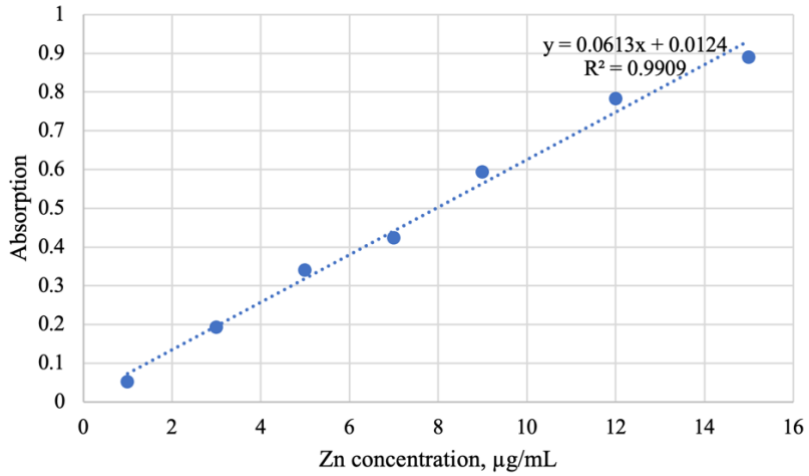

Figure 5. Calibration curve for the determination of Zn.

Accuracy and precision were determined at three concentration levels (1, 7, 15 µg/mL) with five replicates per level. The data was expressed as it described for N-allylimidazole.

Table 5. Accuracy and precision of the AAC method for Zn

Nominal concentration, µg/mL	Measured concentration, µg/mL	Measured concentration, mean, µg/mL	SD (n=5)	RSD, %	Accuracy, %
1.00	0.86	0.91	0.05	5.52	8.69
	0.86				
	0.92				
	0.95				
	0.97				
7.00	7.13	7.41	0.26	3.56	5.85
	7.84				
	7.38				
	7.29				
	7.41				
15.00	15.77	15.67	0.23	1.49	4.46
	15.75				
	15.68				
	15.88				
	15.27				

Pharmacokinetic parameters

To quantify the components of a complex compound in biological samples, HPLC-MSMS and AAS methods were used to determine N-allylimidazole and Zn, respectively. Biological samples from 6 animals for each time point were collected at the following time points after single intraperitoneal administration: 0, 0.083, 0.25, 0.5, 1, 1.5, 2, 3, 4, 6, 24 h and are prepared in accordance with the procedure described above. Tissue concentrations were normalized to organ weight. For this purpose, each measured concentration of the components of the complex compound was converted into the content in the homogenate,

taking into account dilution, and finally presented for calculating pharmacokinetic parameters as the ratio of the component content to the weight of an individual organ. The pharmacokinetic curves and calculated parameters for N-allylimidazole and zinc are shown on Table 6, 7 and Figures 6-8.

Table 6. Pharmacokinetic parameters of N-allylimidazole in plasma and tissues (brain, liver, pancreas, kidneys, and spleen) of BALB/c mice after a single intraperitoneal administration of bis(N-allylimidazole) zinc diacetate (ALL) (25 mg/kg)

Biological sample	Organ weight, g (M ± s.d.)	λz (h^{-1})	C_{max} (ng/mL, plasma; ng/g, tissue*)	T_{max} (h)	$T_{1/2}$ (h)	AUC_{0-t} (ng·h/mL)	$AUC_{0-\infty}$ (ng·h/mL)	MRT_{0-t} (h)	$MRT_{0-\infty}$ (h)
Plasma	-	0.86	1919.96	0.08	0.81	875.56	877.26	0.49	0.5
Kidney	0.24±0.04	0.84	7907.58*	0.25	0.82	8571.87	8702.02	1.07	1.16
Brain	0.37±0.03	0.95	3693.86*	0.25	0.73	4718.97	4753.81	1	1.05
Spleen	0.22±0.07	1.29	4606.19*	0.25	0.54	6736.15	6742.87	0.95	0.96
Liver	0.47±0.14	0.05	959.95*	6	14.5	11168.41	14793.76	10.25	18.74
Pancreas	0.13±0.04	1.37	3661.35*	0.25	0.51	2024.88	2057.64	0.5	0.55

Note: * – recalculated concentrations in tissues, taking into account the dilution during homogenization and normalized to the organs weight.

Table 7. Pharmacokinetic parameters of zinc in plasma and tissues (brain, liver, pancreas, kidneys, and spleen) of BALB/c mice after a single intraperitoneal administration of bis(N-allylimidazole) zinc diacetate (ALL) (25 mg/kg)

Biological sample	Organ weight, g (M ± s.d.)	λz (h^{-1})	Cmax (µg/mL, plasma; µg/g, tissue*)	T_{max} (h)	$T_{1/2}$ (h)	AUC_{0-t} (µg·h/mL)	$AUC_{0-\infty}$ (µg·h/mL)	MRT_{0-t} (h)	$MRT_{0-\infty}$ (h)
Plasma	-	0.18	2.05	1.50	3.78	9.20	9.33	5.00	5.32
Kidney	0.24±0.04	0.24	32.77*	0.25	2.90	175.98	176.81	5.34	5.45
Brain	0.37±0.03	NA	NA	NA	NA	NA	NA	NA	NA
Spleen	0.22±0.07	0.002	54.80*	0.08	NA	343.84	8389.49	10.50	NA
Liver	0.47±0.14	0.04	60.21*	0.25	15.99	273.99	391.65	9.69	20.92
Pancreas	0.13±0.04	0.07	57.52*	1.00	9.69	449.66	540.10	8.14	13.14

Note: * – recalculated concentrations in tissues, taking into account the dilution during homogenization and normalized to the organs weight

Discussion

Given zinc's pivotal role in numerous physiological processes, the development and pharmacological evaluation of zinc-containing compounds continues to attract considerable research interest. Zinc salts are available commercially in multiple formulations. Bis(vinylimidazole) zinc diacetate (Acyzol), formulated for parenteral administration, is used clinically as an antidote for carbon monoxide poisoning and has demonstrated antihypoxic and cardioprotective properties (Aliev et al. 2019). In experimental models of hepatotoxicity, Acyzol reduced the severity of cytolytic, cholestatic, and mesenchymal-inflammatory lesions and supported recovery of hepatic function (Shakhmardanova et al. 2017). Nobelzin® (zinc acetate dihydrate), administered orally as tablets, is approved for the treatment of Wilson's disease, a genetic disorder of impaired hepatic copper excretion, in which it reduces further dietary copper absorption (Weiskirchen 2025). In Japan, the indication for Nobelzin® was expanded in 2017 to include hypozincemia (Ezoe et al. 2024). Early zinc deficiency commonly presents with taste disturbance (dysgeusia); administration of Nobelzin® at 50 mg/day improved taste sensitivity in

patients with dysgeusia and documented hypozincemia after 12 weeks of therapy (Shintani et al. 2023). Despite the availability of effective oral zinc preparations, injectable zinc formulations suitable for correction of zinc deficiency are lacking. The development of parenteral zinc formulations that provide high bioavailability and markedly increase systemic zinc concentrations therefore remains a relevant and timely research objective.

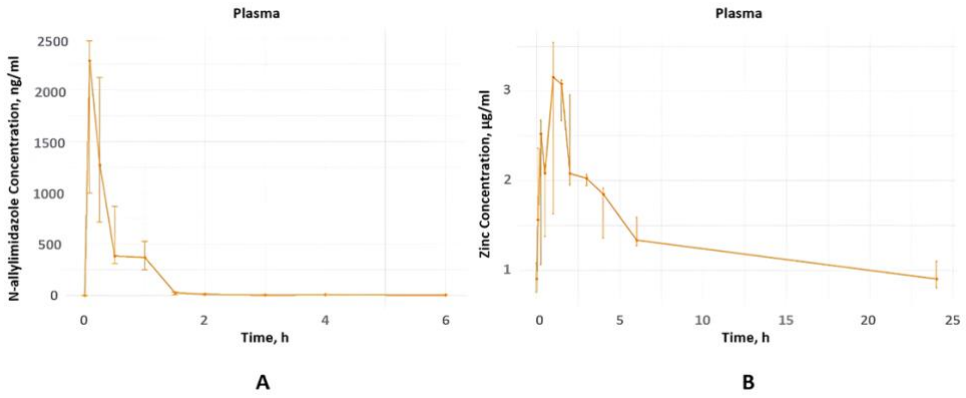

Figure 6. Concentration–time profile of N-allylimidazole (**A**) and Zn (**B**) in plasma.

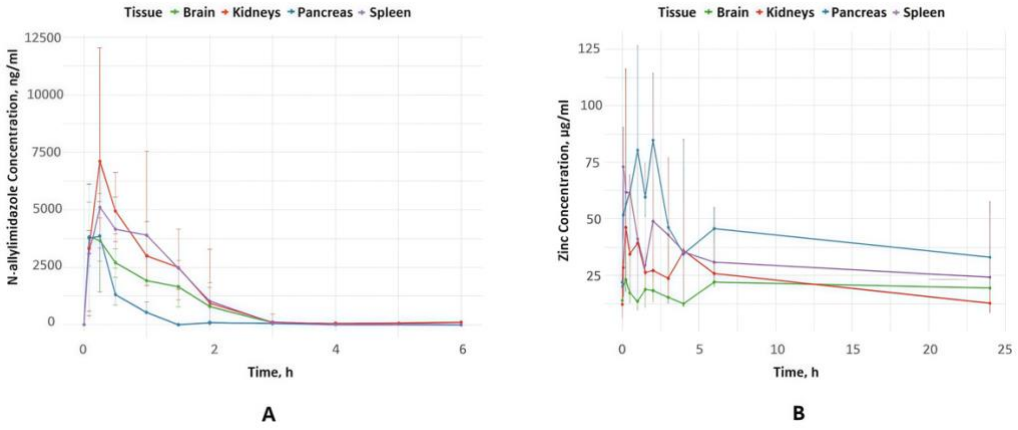

Figure 7. Concentration–time profile of N-allylimidazole (**A**) and Zn (**B**) in brain, kidneys, pancreas, spleen.

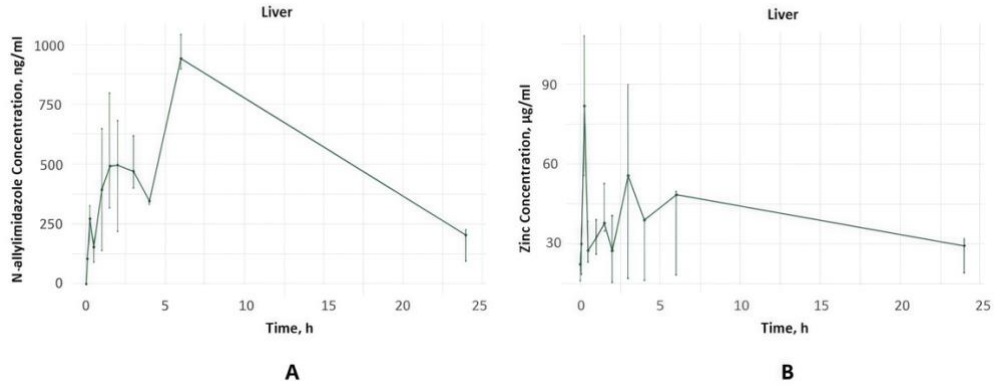

Figure 8. Concentration–time profile of N-allylimidazole (**A**) and Zn (**B**) in liver.

The measured maximal concentrations (C_{max}) of the N-allylimidazole ligand were in the range of 1-8 ppm, which corresponds to a molar value of 9–73 µmol/L (Table 3). The maximal zinc concentrations were in the range of 3–82 ppm, corresponding to 45–1250 µmol/L (Table 4). After subtracting the endogenous zinc level, the C_{max} was in the range of 31–921 µmol/L. Given the initial

molar ligand content of twice that of zinc, there was apparently a significant lack of ligand compared to zinc. One obvious suggestion could be that most of the ligand was in the form of a complex with zinc. The formation constant of the ALL complex from zinc diacetate and ligand in neutral water was calculated to be 370, which is a fairly low value. According to equilibrium, even if all zinc was free, at the maximal zinc concentration in plasma, the complex concentration could only reach 4 x 10^{-6} µmol/L, which is negligible. Acetate anions have an even lower association constant with zinc(II). Thus, the original complex is completely dissociated during biodistribution, due to dilution, at least. However, most zinc is present in plasma as an albumin complex, with a constant formation of about 10^7 (Falcone and Faller 2023). At the endogenous zinc level of 14 µmol/L, the free zinc cation Zn^{2+} in the form of the aqua complex is in the concentration of 2.3 nmol/L, e.g. 0.02% of the total zinc. In other studied organs, the average concentration of free zinc cation (Zn^{2+}) is also at similar low levels, ranging from 0.6 to 2.5 nmol/L (Krezel and Maret 2006). The formation constant of the complex ($[ZnL_2]^{2+}$) of N-allylimidazole (L) with zinc(II) aqua complex (Zn^{2+}) was calculated to be 2.1x10^5. The concentrations of the complexes $[ZnL_2]^{2+}$ and $[ZnL]^{2+}$ in plasma were then calculated and plotted against time (Fig. 9). The concentrations of the complexes are several orders of magnitude lower than the concentrations of the ligand and zinc, and are below the detection limit even at the initial time. The concentration of the monoligated complex is below the nanomolar level, while the concentration of the bisimidazole complex is below the picomolar level. This pattern is also observed in other organs.

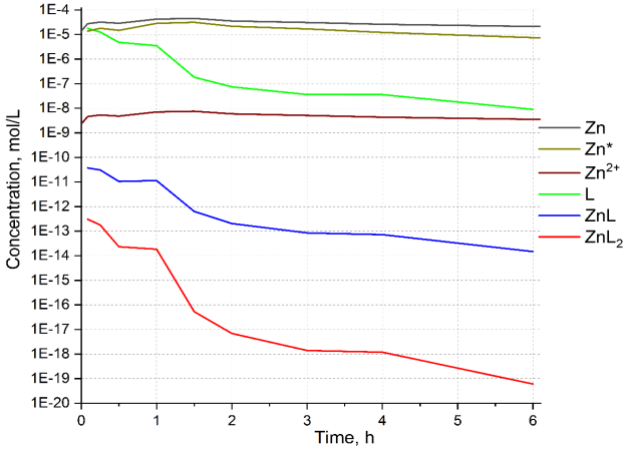

Figure 9. Concentration–time profile of total zinc (Zn), zinc corrected for endogenous level (Zn*), zinc(II) aqua complex (Zn^{2+}), N-allylimidazole (L) and its complexes with aqueous Zn^{2+} (ZnL and ZnL_2) in plasma.

At the beginning, after the administration of the complex ALL, the N-allylimidazole ligand concentration was higher than the total zinc concentration, corrected for the endogenous level (Zn*). Then, the ligand concentration rapidly decreased to zero, while the zinc concentration increased (up to 1.5 h) and then slowly decreased (Fig. 7). The high metabolic rate of N-allylimidazole, compared to zinc, is also confirmed by measurements in other organs studied. N-allylimidazole was detected in all examined biological matrices, including the brain, indicating that the ligand can cross the blood-brain barrier. The T_{max} value was 0.25 h in almost all matrices, consistent with rapid systemic absorption and prompt tissue distribution. The kidneys showed rapid accumulation and very high concentrations (C_{max} 7907.58 µg/g), suggesting renal involvement in ligand elimination, likely in unmetabolized form. In the liver, C_{max} was lower (959.95 µg/g), but the elimination half-life ($T_{1/2}$) was prolonged (14.5 h) and $AUC_{0–24}$ reached 11168.41 µg·h/mL; this reflects a T_{max} of 6 h, whereas ligand concentrations in other organs had already declined to near zero by that time. Together, these parameters indicate slow hepatic accumulation and prolonged retention of N-allylimidazole.

The measured zinc concentrations were consistent with published data. After subtraction of endogenous zinc levels, the highest post-dose concentrations were observed in the liver (60.21 µg/g), pancreas (57.52 µg/g), and spleen (54.80 µg/g). Administration of the ^{68}Zn isotope similarly showed pronounced zinc accumulation in these organs (Yasuno et al. 2011).

The increased zinc content in the liver after intraperitoneal administration of the organic zinc complex may reflect the liver's major role in metal homeostasis, as well as dissociation of the complex in vivo followed by hepatic sequestration of the released zinc ion. The liver may also serve as a primary site of redistribution and transient zinc storage after systemic absorption. The increased zinc content in the spleen may reflect its role as a secondary compartment for zinc redistribution and sequestration after systemic administration. Given the spleen's involvement

in blood filtration and immune cell turnover, this accumulation may also be associated with uptake by reticuloendothelial cells and the physiological demand for zinc in immune processes. The increase in pancreatic zinc content is likely due to both higher bioavailability and efficient tissue delivery, as well as the ability of β-cells to actively accumulate zinc for insulin synthesis and storage (Sisnande et al. 2020). Zinc retention in the pancreas may additionally be supported by zinc transporters, metallothioneins, and the formation of intracellular zinc-containing complexes.

Although N-allylimidazole can cross the BBB, changes in brain zinc concentration were minimal across time points. The BBB tightly regulates the brain microenvironment and maintains zinc homeostasis, so zinc enters the brain mainly through controlled transport systems, including ZIP and ZnT transporters, as well as locally released synaptic zinc. When BBB integrity is compromised, for example during inflammation, trauma, or ischemia, permeability increases and ionic Zn^{2+} may enter brain tissue, where it can exert neurotoxic or modulatory effects (Qi and Liu 2019). The detection of the ligand in the brain, together with the lack of a comparable zinc signal, suggests that the two components may distribute independently *in vivo*. This pattern is consistent with the idea that the organic moiety crosses the blood-brain barrier more readily than zinc, whereas the metal ion remains under tighter homeostatic control and has more restricted CNS entry. However, further studies are needed to clarify the circulating form of zinc and the extent to which complex dissociation contributes to tissue distribution. It should be noted that $AUC_{0-\infty}$ values for the spleen, liver, and pancreas exceeded AUC_{0-24} values, indicating pronounced tropism of the compound for these organs and suggesting that a longer observation period would be needed for trace element levels to return to physiological values. In addition, interanimal variability in endogenous zinc content may have contributed to the results and cannot be fully controlled. Future studies should therefore compare the pharmacokinetics of zinc complexes and zinc salts to better assess the contribution of the organic moiety to the distribution profile of the administered trace element.

Conclusion

The pharmacokinetic analysis demonstrated rapid systemic distribution of N-allylimidazole and zinc after a single intraperitoneal administration of the complex at a dose of 25 mg/kg to BALB/c mice. N-allylimidazole penetrated efficiently into highly perfused tissues, including the brain and kidneys, whereas zinc preferentially accumulated in the liver, pancreas, and spleen. The marked differences in the tissue distribution and metabolic rates of the ligand and zinc, as well as the calculations of equilibrium, suggest a complete dissociation of the complex *in vivo*. Prolonged retention of both components in the liver, along with substantial zinc accumulation in the pancreas and spleen, may be relevant to the biological activity of the compound and warrants further investigation in efficacy studies.

Additional Information

Conflict of interest

The authors declare that they have no conflicts of interest.

Funding

The authors have no funding to report.

Ethics statement

The animal study protocols were approved by the Ethics Committee of Sechenov University (Minutes No. 03-26 of 6 February 2026).

Acknowledgments

The figures were created with BioRender.com.

Data availability

All relevant data generated and analyzed during this study are included in this article

References

- Aliev G, Li Y, Chubarev VN, Lebedeva SA, Parshina LN, Trofimov BA, Sologova SS, Makhmutova A, Avila-Rodriguez MF, Klochkov SG, Galenko-Yaroshevsky PA, Tarasov VV (2019a) Application of acyzol in the context

of zinc deficiency and perspectives. International Journal of Molecular Sciences 20(9): 2104. https://doi.org/10.3390/ijms20092104 [PubMed] [PMC]

- Andreini C, Banci L, Bertini I, Rosato A (2006) Counting the zinc-proteins encoded in the human genome. Journal of Proteome Research 5(1): 196–201. https://doi.org/10.1021/pr050361j [PubMed]
- Brahmachari S, Lee S, Kim S, Yuan C, Karuppagounder SS, Ge P, Shi R, Kim EJ, Liu A, Kim D, Quintin S, Jiang H, Kumar M, Yun SP, Kam T-I, Mao X, Lee Y, Swing DA, Tessarollo L, Ko HS, Dawson VL, Dawson TM (2019) Parkin interacting substrate zinc finger protein 746 is a pathological mediator in Parkinson's disease. Brain: A Journal of Neurology 142(8): 2380–2401. https://doi.org/10.1093/brain/awz172 [PubMed] [PMC]
- Costa MI, Sarmento-Ribeiro AB, Gonçalves AC (2023) Zinc: From biological functions to therapeutic potential. International Journal of Molecular Sciences 24(5): 4822. https://doi.org/10.3390/ijms24054822 [PubMed] [PMC]
- Demirel F, Aksu T, Esen I, Yarali N, Karakaya G, Tunç B (2011) Hypopituitarism masquerading as Prasad's syndrome: A case report. The Turkish Journal of Pediatrics 53(6): 702–704. [PubMed]
- Dong Z, Zhang L, Wang W, Jiang F, Ai H (2023) ZnSO4 protects against premature ovarian failure through PI3K/AKT/GSK3β signaling pathway. Theriogenology 207: 61–71. https://doi.org/10.1016/j.theriogenology.2023.05.023 [PubMed]
- Ezoe S, Ishihara T, Hosogai T, Kokubo T (2024) Post-marketing surveillance of zinc acetate dihydrate for hypozincemia in Japan. Die Pharmazie 79(1): 29–34. https://doi.org/10.1691/ph.2024.3630 [PubMed]
- Falcone E, Faller P (2023) Thermodynamics-based rules of thumb to evaluate the interaction of chelators and kinetically-labile metal ions in blood serum and plasma. Dalton Transactions 52(8): 2197–2208. https://doi.org/10.1039/d2dt03875g [PubMed]
- Galenko-Yaroshevsky PA, Pavlyuchenko II, Shelemekh OV, Trofimov BA, Parshina LN, Popkov VL, Demyanenko SA, Tsymbalov OV, Zadorozhniy AV, Zelenskaya AV, Nektarevskaya IB, Sergeeva AV, Korovaykin NE, Lebedeva SA (2024a) Study of anti-inflammatory, antioxidant, antimicrobial and mineralizing effects of an N-isopropenylimidazole zinc metal complex derivative in experimental endodontic-periodontal lesions in rats. Research Results in Pharmacology 10: 1–13. https://doi.org/10.18413/rrpharmacology.10.515
- Galenko-Yaroshevsky PA, Shelemekh OV, Popkov VL, Zadorozhniy AV, Nektarevskaya IB, Bunyatyan ND, Murashko RA, Lebedeva SA, Zelenskaya AV, Uvarov AV, Gulevskaya ON, Alukhanyan LO, Glechyan TR, Sergeeva AV, Kornetskaya AV, Korovaykin NE (2024b) Study of the anti-inflammatory, analgesic, ulcerogenic and anti-ulcerogenic activity of N-isopropenylimidazole zinc complex derivative. Research Results in Pharmacology 10: 23–43. https://doi.org/10.18413/rrpharmacology.10.443
- Gómez-Zorrilla S, Sendra E, Du J, Espona M, Fierro-Villegas A, Siverio A, Rodriguez-Alarcón A, Castañeda S, López Montesinos I, Plata C, Arrieta-Aldea I, Soldado-Folgado J, García-Giralt N, Vicente R, Güerri-Fernández R (2025) Zinc adjuvant treatment in SARS-CoV-2: A randomized clinical trial. Journal of Trace Elements in Medicine and Biology 92: 127778. https://doi.org/10.1016/j.jtemb.2025.127778 [PubMed]
- Guo J, Yuan Z, Wang R (2024) Zn2+ improves sepsis-induced acute kidney injury by upregulating SIRT7-mediated Parkin acetylation. American Journal of Physiology. Renal Physiology 327(1): F184–F197. https://doi.org/10.1152/ajprenal.00337.2023 [PubMed]
- Hashimoto R, Himoto T, Yamada M, Mimura S, Fujita K, Tani J, Morishita A, Masaki T (2022) Antitumor effect of zinc acetate in hepatocellular carcinoma cell lines via the induction of apoptosis. Journal of Nutritional Science and Vitaminology 68(4): 303–311. https://doi.org/10.3177/jnsv.68.303 [PubMed]
- Hemilä H, Petrus EJ, Fitzgerald JT, Prasad A (2016) Zinc acetate lozenges for treating the common cold: an individual patient data meta-analysis. British Journal of Clinical Pharmacology 82(5): 1393–1398. https://doi.org/10.1111/bcp.13057 [PubMed] [PMC]
- Hou R, He Y, Yan G, Hou S, Xie Z, Liao C (2021) Zinc enzymes in medicinal chemistry. European Journal of Medicinal Chemistry 226: 113877. https://doi.org/10.1016/j.ejmech.2021.113877 [PubMed]
- Jiang H, Yang B, Wang F, Li K, Zhu Y, Liu B, Ren H, Tian S, Xu Y, Pang A, Yang X (2021) Association of single nucleotide polymorphism at rs2275294 in the ZNF512B gene with prognosis in amyotrophic lateral sclerosis. Neuromolecular Medicine 23(2): 242–246. https://doi.org/10.1007/s12017-020-08634-y [PubMed]
- Kanda T, Sasaki-Tanaka R, Abe H, Yokoo T, Sakamaki A, Hayashi K, Kamimura H, Tsuchiya A, Masuzaki R, Kogure H, Okamoto H, Terai S (2025) Zinc acetate inhibits hepatitis a virus replication: Possible treatment for patients with type A acute-on-chronic liver failure. Pathogens 14(9): 882. https://doi.org/10.3390/pathogens14090882 [PubMed] [PMC]
- Kimura T, Kambe T (2016) The functions of metallothionein and ZIP and ZnT transporters: An overview and perspective. International Journal of Molecular Sciences 17(3): 336. https://doi.org/10.3390/ijms17030336 [PubMed] [PMC]
- Kocyła A, Adamczyk J, Krężel A (2018) Interdependence of free zinc changes and protein complex assembly - insights into zinc signal regulation. Metallomics 10(1): 120–131. https://doi.org/10.1039/c7mt00301c [PubMed]
- Krezel A, Maret W (2006) Zinc-buffering capacity of a eukaryotic cell at physiological pZn. Journal of Biological Inorganic Chemistry 11(8): 1049–1062. https://doi.org/10.1007/s00775-006-0150-5 [PubMed] [PMC]
- Lebedeva SA, Galenko-Yaroshevsky (Jr.) PA, Fateeva TV, Pashin SS, Pashina NR, Nektarevskaya IB, Zadorozhniy AV, Shelemekh OV, Ravaeva MY, Chuyan EN, Alukhanyan LO, Glechyan TR, Mutig K, Materenchuk MY (2023) Effective wound healing agents based on N-alkenylimidazole zinc complexes derivatives: future prospects and opportunities. Research Results in Pharmacology 9: 27–39. https://doi.org/10.18413/rrpharmacology.9.10047
- Liang Y, Li Q, Chen K, Ni W, Zhan Z, Ye F, Li Y, Fang Y, Zhang F, Chen L, Ding Y (2017) Zinc finger protein 307 functions as a tumor-suppressor and inhibits cell proliferation by inducing apoptosis in hepatocellular carcinoma. Oncology Reports 38(4): 2229–2236. https://doi.org/10.3892/or.2017.5868 [PubMed]
- Lin P-H, Sermersheim M, Li H, Lee PHU, Steinberg SM, Ma J (2017) Zinc in wound healing modulation. Nutrients 10(1): 16. https://doi.org/10.3390/nu10010016 [PubMed] [PMC]
- Matowane GR, Mashele SS, Makhafola TJ, Chukwuma CI (2023) The ameliorative effect of zinc acetate with caffeic acid in the animal model of type 2 diabetes. Biomedicine & Pharmacotherapy 163: 114779. https://doi.org/10.1016/j.biopha.2023.114779 [PubMed]
- Miroshnikov SA, Skalny AV, Zavyalov OA, Frolov AN, Grabeklis AR (2020) The reference values of hair content of trace elements in dairy cows of Holstein breed. Biological Trace Element Research 194(1): 145–151. https://doi.org/10.1007/s12011-019-01768-6 [PubMed]

- Park S, Hwang Y, Eom KS, Cheong JS, Lee SJ (2025) Controlling gene expression through five zinc finger domains of ZNF18. Protein Science 34(9): e70278. https://doi.org/10.1002/pro.70278 [PubMed] [PMC]
- Parshina LN, Grishchenko LA, Smirnov VI, Borodina TN, Shakhmardanova SA, Tarasov VV, Apartsin KA, Kireeva VV, Trofimov BA (2019) Synthesis, characterization and biological evaluation of Zn(II) and Co(II) complexes of N-allylimidazole as potential hypoxia-targeting agents. Polyhedron 161: 126–131. https://doi.org/10.1016/j.poly.2019.01.005
- Qi Z, Liu KJ (2019) The interaction of zinc and the blood-brain barrier under physiological and ischemic conditions. Toxicology and Applied Pharmacology 364: 114–119. https://doi.org/10.1016/j.taap.2018.12.018 [PubMed] [PMC]
- Qian Y, Wu Q (2025) The multifaceted roles of zinc finger proteins in pluripotency and reprogramming. International Journal of Molecular Sciences 26(11): 5106. https://doi.org/10.3390/ijms26115106 [PubMed] [PMC]
- Shakhmardanova SA, Galenko-Yaroshevskii PA (2017) N-alkenylimidazole metal complex derivatives as effective agents for the hypoxic conditions. Research Results in Pharmacology 9(3): 49–72. https://doi.org/10.18413/rrpharmacology.9.10047
- Shakhmardanova SA, Babaniyazova ZH, Tarasov VV, Pevnev GO, Chubarev VN, Sologova SS (2017) Protective effect of acyzol in a model of carbon tetrachloride-induced hepatotoxicity. BioNanoScience 7: 329–332. https://doi.org/10.1007/s12668-016-0352-4
- Shintani T, Ohta K, Ando T, Hayashido Y, Yanamoto S, Kajiya M, Shiba H (2023) Retrospective study on the therapeutic efficacy of zinc acetate hydrate administration to patients with hypozincemia-induced dysgeusia. BMC Oral Health 23(1): 159. https://doi.org/10.1186/s12903-023-02866-7 [PubMed] [PMC]
- Sisnande T, Lima CK, da Silva DC, Beninatto TM, Alves NL, Amaral MJ, Miranda-Alves L, Lima LMTR (2020) Dietary zinc restriction promotes degeneration of the endocrine pancreas in mice. Biochimica Et Biophysica Acta. Molecular Basis of Disease 1866(5): 165675. https://doi.org/10.1016/j.bbadis.2020.165675 [PubMed]
- Skalny AV, Sotnikova TI, Korobeynikova TV, Tinkov AA (2022) Significance of zinc deficiency correction for practical medicine: a review. Sechenov Medical Journal 13: 4–17. https://doi.org/10.47093/2218-7332.2022.13.4.4-17
- Stiles LI, Ferrao K, Mehta KJ (2024) Role of zinc in health and disease. Clinical and Experimental Medicine 24(1): 38. https://doi.org/10.1007/s10238-024-01302-6 [PubMed] [PMC]
- Thompson MW (2022) Regulation of zinc-dependent enzymes by metal carrier proteins. Biometals 35(2): 187–213. https://doi.org/10.1007/s10534-022-00373-w [PubMed] [PMC]
- Tyurin VS, Babasieva VS, Grigoriev MS, Parshina LN, Zamilatskov IA, Smolyarchuk EA, Nesterova OV, Turenko VN, Kolyganova TI, Arzumanian VG, Mutig K, Samsonov MY, Lebedeva SA (2026) Complexes of zinc(II) chloride with N-vinyl-, N-allyl- and N-propargylimidazoles: Structural, theoretical and biological studies. Pharmaceuticals 19(6): 874. https://doi.org/10.3390/ph19060874 [PubMed] [PMC]
- Wegmüller R, Tay F, Zeder C, Brnic M, Hurrell RF (2014) Zinc absorption by young adults from supplemental zinc citrate is comparable with that from zinc gluconate and higher than from zinc oxide. The Journal of Nutrition 144(2): 132–136. https://doi.org/10.3945/jn.113.181487 [PubMed] [PMC]
- Weiskirchen R (2025) Comprehensive pharmacological management of Wilson's disease: Mechanisms, clinical strategies, and emerging therapeutic innovations. Sci 7: 94. https://doi.org/10.3390/sci7030094
- Yasuno T, Okamoto H, Nagai M, Kimura S, Yamamoto T, Nagano K, Furubayashi T, Yoshikawa Y, Yasui H, Katsumi H, Sakane T, Yamamoto A (2011) The disposition and intestinal absorption of zinc in rats. European Journal of Pharmaceutical Sciences 44(3): 410–415. https://doi.org/10.1016/j.ejps.2011.08.024 [PubMed]
- Yu X, Chen X, Wu W, Tang H, Su Y, Lian G, Zhang Y, Xie L (2025) Zinc Alleviates diabetic muscle atrophy via modulation of the SIRT1/FoxO1 autophagy pathway through GPR39. Journal of Cachexia, Sarcopenia and Muscle 16: e13771. https://doi.org/10.1002/jcsm.13771 [PubMed] [PMC]

Author Contribution

- **Victoria S. Babasieva**, PhD student, Institute of Pharmacy, Sechenov First Moscow State Medical University (Sechenov University), Moscow, Russia; e-mail: victoriababasieva@mail.ru; **ORCID ID:** https://orcid.org/0000-0003-2846-4133. Conceptualization, Investigation, Methodology, Project Administration, Writing – Original Draft.
- **Vladislav N. Turenko**, junior researcher, Institute of Pharmacy, Sechenov First Moscow State Medical University (Sechenov University), Moscow, Russia; Allergy and Immunology Research Centre FMBA of Russia, Moscow, Russia; e-mail: vladislav.turenko.n@gmail.com; **ORCID ID:** https://orcid.org/0000-0003-1817-0844. Conceptualization, Investigation, Methodology, Validation, Writing – Original Draft.
- **Andrey R. Grabeklis**, Senior researcher, People's Friendship University of Russia named after Patrice Lumumba (RUDN University), Moscow, Russia; e-mail: grabeklis-ar@rudn.ru; **ORCID ID:** https://orcid.org/0000-0003-4017-4139. Supervision.
- **Dmitry M. Lyapunovsky**, PhD student, People's Friendship University of Russia named after Patrice Lumumba (RUDN University), Moscow, Russia; e-mail: lyapunovskiy-dm@rudn.ru; **ORCID ID:** https://orcid.org/0009-0003-4863-1792. Investigation, Methodology.
- **Anatoly V. Skalny**, MD, PhD, Head of Department at Peoples' Friendship University of Russia, People's Friendship University of Russia named after Patrice Lumumba (RUDN

University), Moscow, Russia; e-mail: skalnyy-av@rudn.ru; **ORCID ID:** https://orcid.org/0000-0001-7838-1366. Supervision.

- **Vladimir S. Tyurin**, Senior researcher, Frumkin Institute of Physical Chemistry and Electrochemistry, Russian Academy of Sciences, Moscow, Russia; e-mail: tv@org.chem.msu.ru; **ORCID ID:** https://orcid.org/0000-0002-8663-2935. Formal Analysis, Writing – Review & Editing.
- **David E. Bagaev**, Junior researcher, Institute of Pharmacy, Sechenov First Moscow State Medical University (Sechenov University), Moscow, Russia; Allergy and Immunology Research Centre FMBA of Russia, Moscow, Russia; e-mail: bagaev3411302@mail.ru; **ORCID ID:** https://orcid.org/0009-0008-5495-7939. Investigation.
- **Victoria G. Krasnyanskaya**, laboratory assistant, Allergy and Immunology Research Centre FMBA of Russia, Moscow, Russia; e-mail: lec@nrcii.ru; **ORCID ID:** https://orcid.org/0000-0001-7604-8172. Investigation.
- **Galina F. Vasilenko**, researcher, Allergy and Immunology Research Centre FMBA of Russia, Moscow, Russia; e-mail: lec@nrcii.ru; **ORCID ID:** https://orcid.org/0000-0001-7940-1664. Investigation.
- **Obinna Ikebunwa**, PhD student, Institute of Pharmacy, Sechenov First Moscow State Medical University (Sechenov University), Moscow, Russia; Department of Pharmacology and Toxicology, Michigan State University, Michigan, USA; e-mail: ikebunwaobinna@gmail.com; **ORCID ID:** https://orcid.org/0009-0006-5619-5531. Investigation, Data Curation.
- **Valery V. Smirnov**, Dr. Sci, Professor, Institute of Pharmacy, Sechenov First Moscow State Medical University (Sechenov University), Moscow, Russia; Allergy and Immunology Research Centre FMBA of Russia, Moscow, Russia; e-mail: vall@mail.mipt.ru; **ORCID ID:** https://orcid.org/0000-0002-8232-6682. Supervision.
- **Svetlana A. Lebedeva**, Dr. Sci, Professor, Institute of Pharmacy, Sechenov First Moscow State Medical University (Sechenov University), Moscow, Russia; People's Friendship University of Russia named after Patrice Lumumba (RUDN University), Moscow, Russia; Scientific Center of Genetics and Life Sciences, Sirius University of Science and Technology, Sirius, Russia; e-mail: Lebedeva502@yandex.ru; **ORCID ID:** https://orcid.org/0000-0001-8769-1040. Supervision, Visualization, Writing – Review & Editing.